UDK 546.664:537.226.86
Original scientific article/Izvirni znanstveni članek

ISSN 1580-2949
Mater. Tehnol.

THERMAL DEFORMATION BEHAVIOR OF HIGH-PURITY RARE EARTH METAL DYSPROSIUM

OBNAŠANJE ZELO ČISTEGA REDKOZEMELJSKEGA KOVINSKEGA DISPROZIJA MED TERMIČNO DEFORMACIJO

Haishuang Lv[1], Yanmei Li[1*], Dounan Chen[2], Guohuai Liu[1], Rui Liu[1], Zhaodong Wang[1]

[1]The State Key Laboratory of Rolling and Automation, Northeastern University, Shenyang 110819, China
[2]Materials Science and Engineering, Northeastern University, Shenyang 110819, China

Prejem rokopisa – received: 2024-02-23; sprejem za objavo – accepted for publication: 2024-12-05

doi:10.17222/mit.2024.1115

High-purity rare earth metal dysprosium was subjected to a single-pass thermal compression test at temperatures ranging from 300 °C to 700 °C and strain rates ranging from 0.1 s^{-1} to 10 s^{-1} using an MMS-200 thermal simulation testing machine. The true stress-strain curves, macro and microstructure of dysprosium were analyzed, leading to the establishment of processing maps and constitutive equation for dysprosium. Results revealed that the stress of dysprosium decreased with increasing deformation temperature and decreasing strain rate. Moreover, as the strain rate reached 5 s^{-1}, the stress-strain curve gradually transitioned from dynamic recovery to dynamic recrystallization, with a more pronounced softening behavior observed at higher strain rates. Based on the processing diagram and sample microstructure analysis, it was determined that the optimal deformation range for dysprosium is between 350 °C and 500 °C at a strain rate of 1–10 s^{-1}.

Keywords: dysprosium, hot deformation behavior, stress-strain curve, processing maps

Avtorji v članku opisujejo raziskavo v kateri so zelo čist kovinski redkozemeljski disprozij v enem koraku termično tlačno deformirali v temperaturnem območju med 300 °C to 700 °C, pri hitrostih deformacije 0,1 s^{-1} do 10 s^{-1} na preizkuševalnem termičnem simulatorju MMS-200. Avtoriji so analizirali makro in mikrostrukturo ter izdelali prave krivulje napetost-deformacija deformiranega disprozija. S pomočjo le-teh so nato lahko izdelali procesne mape in razvili konstitutivni model deformacije disprozija. Rezultati raziskave so pokazali, da napetost potrebna za deformacijo disprozija pada z naraščanjem temperature deformacije in zmanjševanjem hitrosti deformacije. Nadalje, ko so avtorji dosegli hitrost deformacije 5 s^{-1} je krivulja napetost-deformacija postopoma prehajala iz oblike značilne za popravo v obliko značilno za dinamično rekristalizacijo z bolj izrazitim mehčanjem pri visokih hitrostih deformacije. Na osnovi procesnega diagrama in analiz mikrostrukture so ugotovili, da je optimalno območje deformacije disprozija med 350 °C in 500 °C pri deformacijskih hitrostih od 1 s^{-1} do 10 s^{-1}.

Ključne besede: disprozij, obnašanje med vročo deformacijo, krivulja *napetost-deformacija*, procesne mape

1 INTRODUCTION

Sputtered thin-film materials, high-purity rare earth metals, and alloy targets have emerged as crucial core materials for numerous rare earth functional materials and their devices. These are extensively utilized in high-tech industries such as national defense, military industry, new energy vehicles, integrated circuit chips, etc., providing vital support for high-tech industrial innovation.[1] Dysprosium, a rare earth metal with excellent thermal absorption cross-section and favorable mechanical properties, finds wide applications in atomic energy, aerospace, electronics, magnetic materials, and other fields. However, due to its susceptibility to air reaction at high temperatures along with its highly active nature and close-packed hexagonal crystal structure, rolling often leads to poor plasticity resulting in surface cracks and edge cracks. This poses challenges during processing while also causng significant surface oxidation loss leading to resource wastage. The currently available literature on the deformation behavior of dysprosium is limited, which hampers the formulation of a reasonable deformation technology for dysprosium. By conducting thermal simulation compression experiments using different deformation processes it is possible to obtain true stress-true strain curves of dysprosium enabling the derivation of a thermal deformation constitutive equation that can be used to construct a processing map, thereby enhancing our understanding of this rare earth material.

Wang Yong et al.[2] investigated the high-temperature compression deformation behavior of cast Mg-4.3Y-3.3Nd-0.6Zr alloy using a Gleeble-1500D thermal simulation machine, providing essential reference for high-temperature extrusion of the alloy. Ding Rongrong et al.[3] examined the deformation behavior of Ti-5Al-5Mo-5V-1Cr-1Fe alloy samples under different deformation processes through hot compression tests conducted on a Gleeble 3500 thermal simulation testing machine. They determined the optimal range of process parame-

*Corresponding author's e-mail:
liym@ral.neu.edu.cn (Yanmei Li)

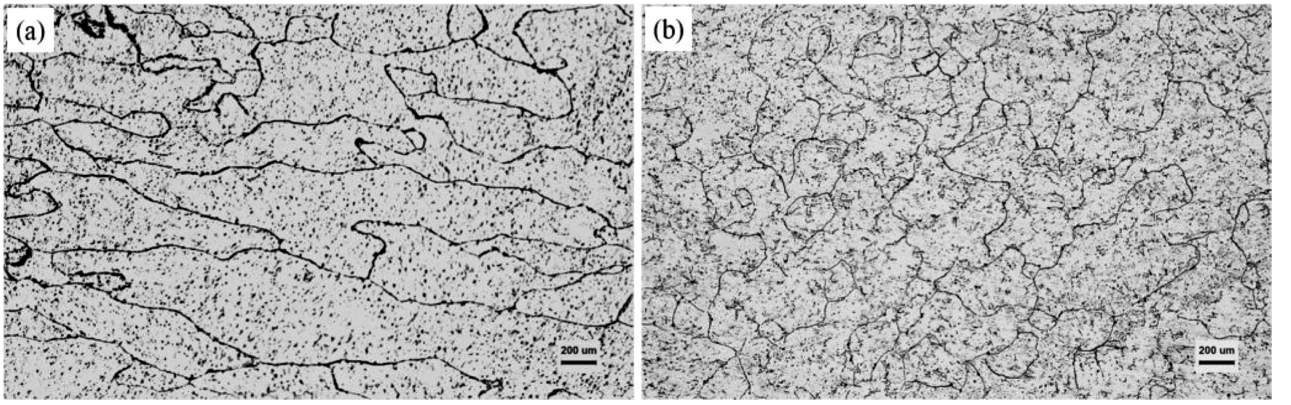

Figure 1: Metallographic microstructure of as-cast dysprosium: a) columnar grain, b) equiaxed grain

ters for high-temperature deformation of this alloy, thus providing necessary experimental data for finite element numerical simulation of forging and formulation of process parameters. H. Wu et al.[4] performed an isothermal compression test on a new Al-Zn-Mg-Er-Zr alloy using a Gleeble 3800 thermal simulation test machine to investigate its deformation behavior and related microstructure evolution during high-temperature deformation, thereby providing crucial experimental data for formulating deformation process parameters for this particular alloy. Yao Weiyi et al.[5] conducted a series of isothermal compression experiments on rolled 7050Al alloy at different temperatures and strain rates to analyze the thermoplastic deformation behavior and microstructure evolution in this high-strength aluminum alloy, which is of significant importance for achieving ideal products. Liu Linxi et al.[6,7] elucidated the importance of various deformation degrees and temperatures for the microstructure evolution, precipitation behavior and mechanical responses of 9Cr3Co3W1Cu ferritic/martensitic steel.

The Arrhenius-type constitutive model, Johnson-Cook model, Zerilli-Armstrong model, Fiels-Backofen model[8–11] and other models have been proposed to describe the constitutive behavior of metal alloys. Additionally, the influence of microstructure evolution on the flow stress during thermal deformation has also been estimated. Among these models, the Arrhenius-type constitutive model effectively captures the flow stress behavior across a wide range.[12] Therefore, we employed this model to establish the relationships between flow stress and strain, strain rate, and deformation temperature for dysprosium. Furthermore, we investigated the microstructure characteristics in both stable and unstable regions of the hot working diagram while elucidating the mechanism behind the microstructure evolution during thermal deformation. These findings have significant implications for comprehending the thermal deformation behavior of dysprosium, optimizing the thermal processing technology, as well as enhancing the processing quality and efficiency of dysprosium products.

2 EXPERIMENTAL PART

The raw material for this experimental study was a high-purity (3N) rare earth metal dysprosium cast billet measuring 200 × 200 × 40 mm. Dysprosium has a soft texture with a microhardness of 66.2 HV. The as-cast microstructure of metallic dysprosium, as depicted in **Figure 1**, consisted of two distinct grain types: columnar grains (**Figure 1a**) and equiaxed grains (**Figure 1b**). The perimeter was characterized by a thin layer of columnar grains, while the center was occupied by a region of equiaxed grains with varying sizes. Specifically, the equiaxed grains exhibited dimensions ranging from 100 μm to 500 μm. In contrast, the columnar grains adopted an elongated, columnar morphology, with short axes measuring between 80 μm and 600 μm and long axes spanning from 200 μm to 3 mm, with uneven grain sizes. Cylindrical as-cast specimens, measuring (8 × 15) mm, were subjected to a single-pass compression heat simulation experiment on the MMS-200 thermal simulation testing machine at varying deformation temperatures and rates, as illustrated in **Figure 2**. The specimens were subsequently cut longitudinally, and after inlaying, grinding, and etching, the microstructure was examined.

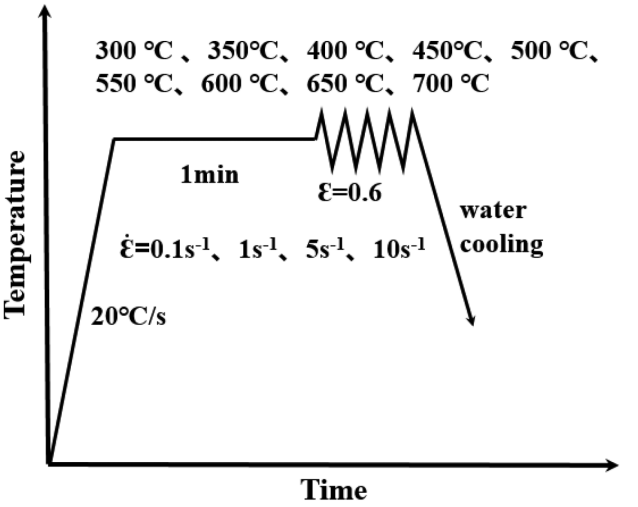

Figure 2: Single-pass compression thermal simulation process

3 RESULTS AND DISCUSSION

3.1 Influence of deformation process parameters on the flow stress

During plastic deformation of metal materials at high temperatures, there are simultaneous processes including work hardening caused by a strain increase and softening caused by dynamic recovery and dynamic recrystallization. A deformation process generally consists of two stages: non-steady state (transitional state) and steady state deformation. Thermal compression is controlled by thermal activation, and its stress magnitude is affected by the dislocation configuration within the deformed body. At the beginning of deformation, a dislocation source is activated, resulting in an increase in dislocation density, so the stress rapidly increases. In the later stage of deformation, as the strain increases, the stress curve tends to balance, and the softening mechanisms such as dynamic recovery and dynamic recrystallization cause the softening and work hardening to reach a dynamic equilibrium, and deformation tends to stabilize.

There are two types of rheological stress curves under different processes: dynamic recovery and dynamic recrystallization, as shown in **Figure 3**. The curve tends to stabilize after the true strain reaches 0.4. As the strain rate increases to 5 s^{-1}, the curve gradually transitions from dynamic recovery to dynamic recrystallization. At the beginning of deformation, the stress increases linearly with the increase in the strain, and the curve is a straight line with a large slope, indicating significant work hardening. As deformation progresses, the rate of stress increase begins to decrease, but it remains on an upward trend until it reaches the peak stress, where the curve exhibits a slope that gradually decreases but remains greater than zero. At this point, work hardening, dynamic recovery, and dynamic recrystallization occur simultaneously, but work hardening dominates. When the deformation is sufficiently large, the rheological stress remains at a stable value with the increase in the strain, and the slope of the curve is approximately equal to zero, entering the steady-state deformation stage. At this point, the curve exhibits complete dynamic recovery or recrystallization.[13] Under each strain rate condition, dysprosium undergoes varying degrees of stress softening, and this softening behavior becomes more pronounced as the strain rate increases. This is similar to the principle found in high-purity fine-grained titanium.[14]

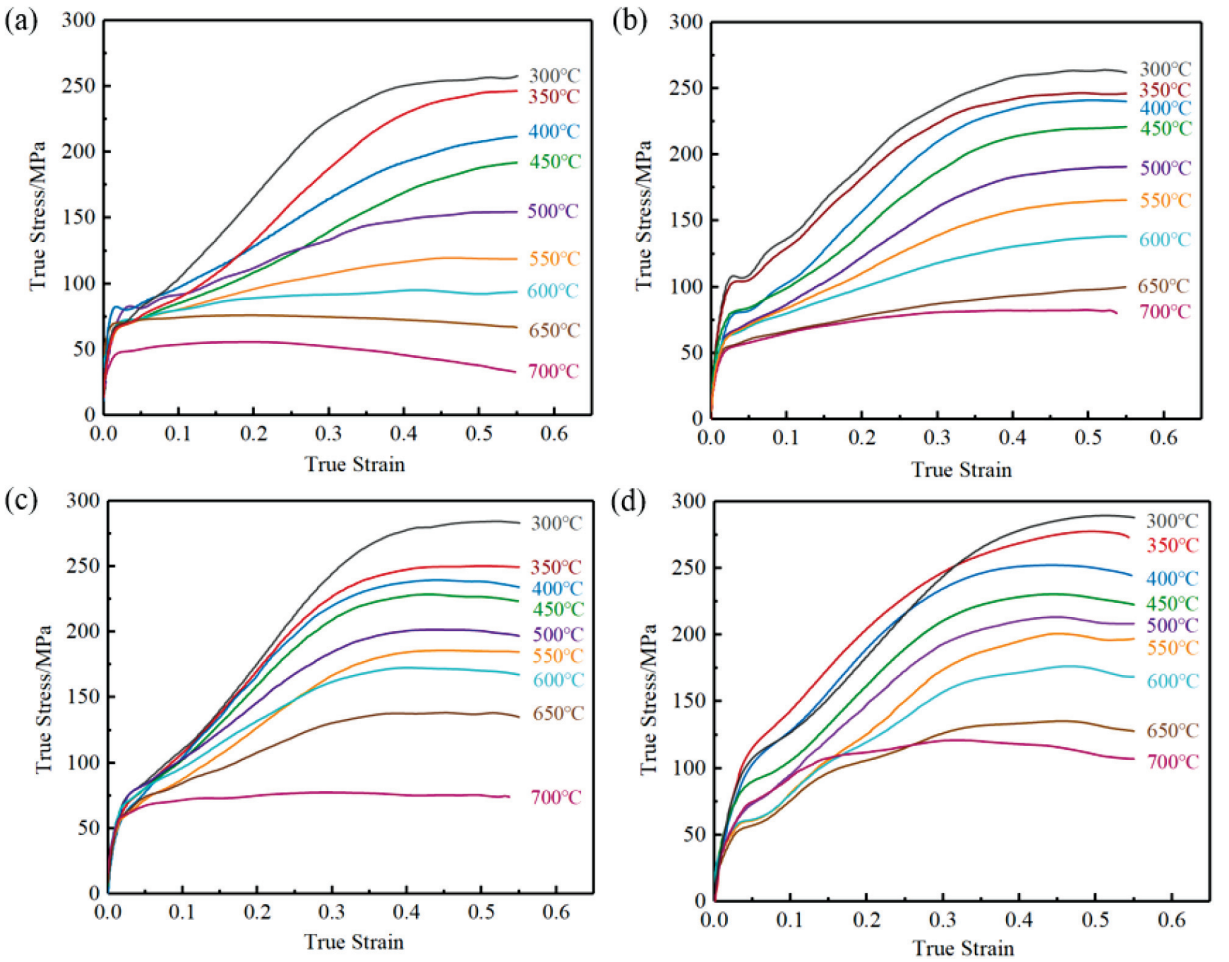

Figure 3: Rheological stress curves of dysprosium at different temperatures: a) 0.1 s^{-1}, b) 1 s^{-1}, c) 5 s^{-1}, d) 10 s^{-1}

3.2 Processing maps and analysis of thermal deformation behavior of corresponding zones

In order to better analyze and predict the processing capability of metallic materials during high-temperature processing, constructing a processing map based on different deformation parameters is an effective approach. Results of a processing map can intuitively reflect the states of the stable and unstable zones, which can assist in determining the reasonable hot processing parameters suitable for the experimental materials. Moreover, it can reflect different deformation mechanisms of the material in the hot processing zone, thereby guiding the actual production process. Common deformation mechanisms in the safe processing zone include dynamic recovery and dynamic recrystallization, while in the unstable zone, common deformation mechanisms include flow localization, intense deformation zones, and cracks. In order to obtain the necessary microstructure for good control of mechanical properties, it is essential to explore the process parameters during processing. According to the Dynamic Material Model (DMM) proposed by Prasad et al., when a metal undergoes hot processing, it obtains strain energy storage during compression deformation. At this time, the dynamic constitutive relationship obtained under deformation conditions can be described with Equation (1).

$$\sigma = k\dot{\varepsilon}^{\mathrm{m}} \tag{1}$$

In the above equation, k is the stress coefficient and m is the strain rate sensitivity coefficient.

In hot deformation, the total input energy is represented by P. There are two ways of consuming this energy: one is deformation heat dissipation G, and the other is energy consumption J through microstructural transformations in the form of work hardening, recovery, and recrystallization. The relationship between them is shown in Equation (2):

$$P = \sigma\dot{\varepsilon} = \int_0^{\dot{\varepsilon}} \sigma \mathrm{d}\dot{\varepsilon} + \int_0^{\sigma} \sigma \mathrm{d}\dot{\varepsilon} = G + J \tag{2}$$

In order to study these two types of energy consumption, the relationship between the strain rate sensitivity coefficient m and the power dissipation efficiency η can be expressed with Equation (3):

$$\eta = \frac{2m}{m+1} \tag{3}$$

When processing the data, the third derivative of the stress strain rate of the material is used for fitting, as it can ensure the accuracy of the calculation to the greatest extent. Therefore, the strain rate sensitivity coefficient m can be represented by Equation (4):

$$m = \frac{\partial \ln \sigma}{\partial \ln \dot{\varepsilon}} = b + 2c \ln \dot{\varepsilon} + 3d(\ln \dot{\varepsilon})^2 \tag{4}$$

During the high-temperature rolling process, the extent of dynamic recrystallization of the metal during deformation is closely related to the material's energy consumption during thermal deformation. The larger the energy consumption factor, the more complete is dynamic recrystallization, and the finer are the equiaxed grains obtained. According to the principle of maximum entropy, when a metal undergoes continuous large plastic deformation, the criterion for whether the material becomes unstable can be expressed with dimensionless rheological instability coefficient $\xi(\dot{\varepsilon})$, as shown in Equation (5).

$$\xi(\dot{\varepsilon}) = \frac{\partial \ln(m/m+1)}{\partial \ln \dot{\varepsilon}} + m < 0 \tag{5}$$

The values of η and $\xi(\dot{\varepsilon})$ are obtained from the above calculations. Based on the Prasad criterion, a power dissipation map and a flow instability map can be constructed by varying the strain rate and deformation temperature. Therefore, by combining the power dissipation map and the flow instability map, a processing map of true strain in a range of 0.2≈0.5 is obtained by overlaying the two maps, as shown in **Figure 4**.

In **Figure 4**, the shaded area of the processing map represents the unstable zone, which mainly appears in the low-temperature and low strain rate zone (lower left) and the high-temperature and high strain rate zone (upper right). As the strain increases, the unstable zone on the left expands to the right, and the unstable zone in the upper right expands downward. When deformation reaches 0.5, the area of the unstable zone is the largest, indicating that the instability mechanism of dysprosium is sensitive to strain, and the strain affects the instability mechanism under different deformation processes differently. Distribution of the unstable zone can provide a theoretical basis for the regulation of microstructural uniformity and the formulation of hot processing technology, but it cannot be the sole criterion for determining safe and unstable zones during hot processing. It also needs to be further assessed in conjunction with the power dissipation map.

Macro-distribution characteristics of the power dissipation map basically do not change with the change in the strain, indicating that the transient process during hot processing is steady. The power dissipation factor η gradually increases with the increase in the deformation temperature and the decrease in the strain rate. When the deformation is 0.5, under the conditions of high deformation temperature and high strain rate, the system introduces the highest input energy, and $\eta_{\max}$ is about 0.74. Specifically, when the deformation is set to 0.2, although the input power peak is lower than other large deformations, the η at low-temperature deformation is the highest. By comparing it with the unstable zone, we can see that the deformation of 0.2 offers the widest selection area of deformation parameters. Usually, a higher power dissipation factor means that the material exhibits better processability under this deformation condition. It may be more likely to undergo dynamic rheological softening, and even show superplasticity. However, when the η

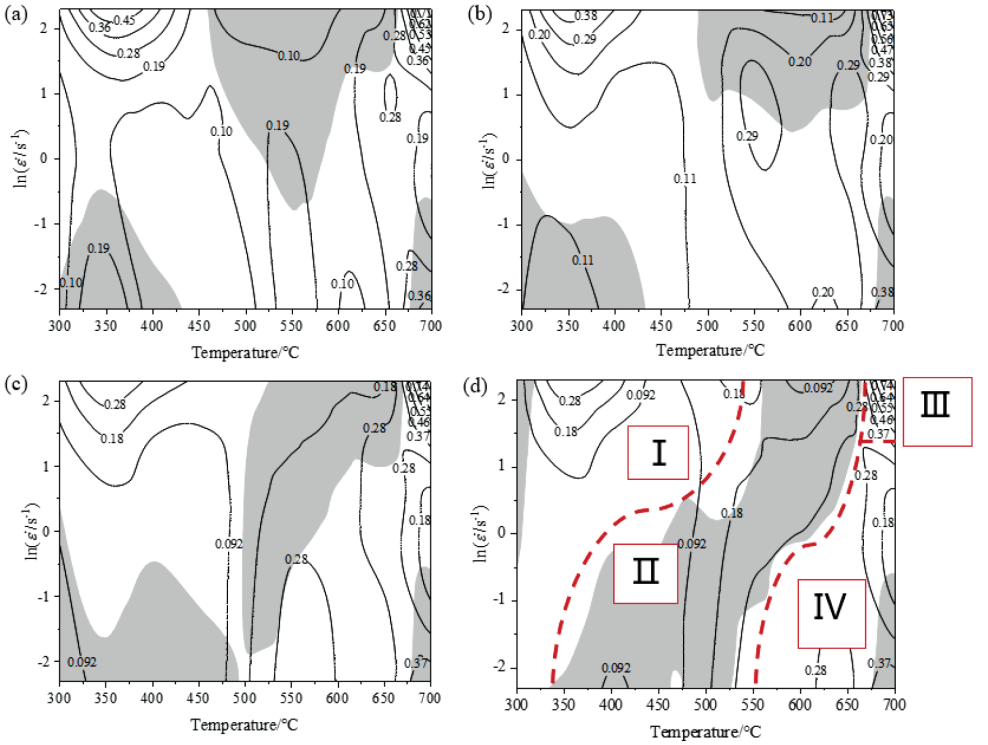

Figure 4: Processing maps of dysprosium: a) ε = 0.2, b) ε = 0.3, c) ε = 0.4, d) ε = 0.5

value is too high, the input of external energy may cause a plastic flow of the structure or material failure (such as the generation of cracks or holes, the formation of adiabatic shear bands, etc.); therefore, we need to further assess the hot processing window of the alloy in conjunction with the microstructure.[13]

3.3 Effects of deformation process parameters on the microstructure of material

The microstructure after hot deformation under different processes is shown in **Figure 5**. The grains in the material structure are elongated perpendicular to the di-

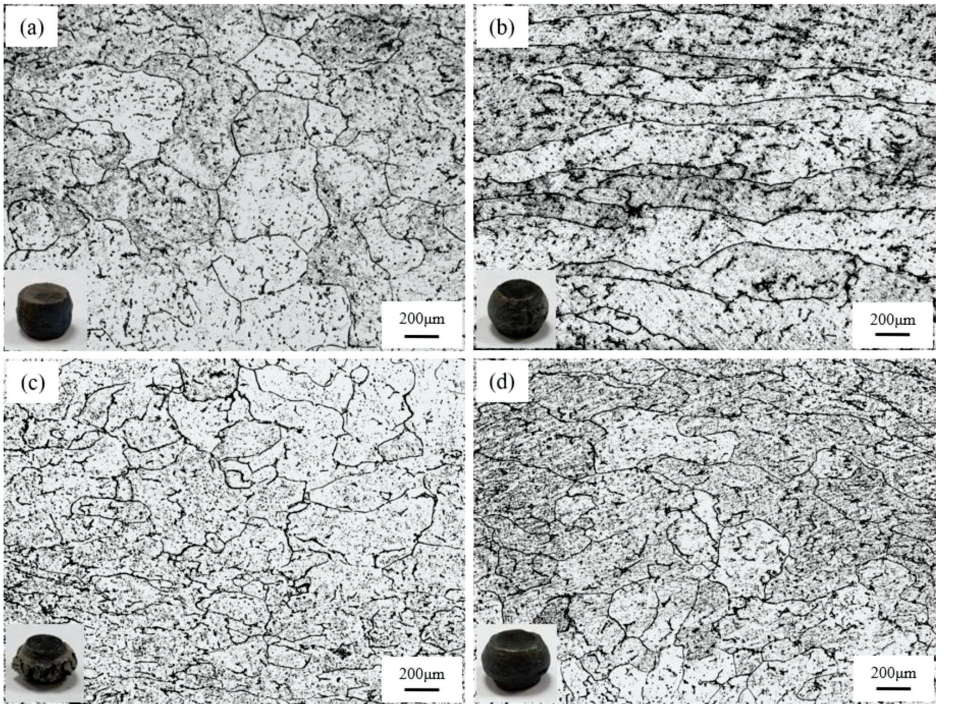

Figure 5: Microstructure after thermal deformation under different processes: a) 400 °C-10 s^{-1}, b) 500 °C-1 s^{-1}, c) 700 °C-10 s^{-1}, d) 650 °C-5 s^{-1}

rection of compression, and small recrystallized grains appear near the grain boundaries of large grains in the structure under high strain rate deformation process. Region I in the processing map corresponds to 400 °C-10 s^{-1}, where the structure is mainly recrystallized grains, with no obvious elongated deformed grains; Region II in the processing map corresponds to 500 °C-1 s^{-1}, which is the unstable zone, where the structure shows uneven deformation and abnormally large phenomena; Region III in the processing map corresponds to 700 °C-10 s^{-1}, where the internal structure deforms unevenly, and recrystallized grains coexist with elongated grains in the direction perpendicular to the deformation and other directions; Region IV in the processing map corresponds to 650 °C-5 s^{-1}, where recrystallized grains and deformed elongated grains coexist in the structure. The best processing area provided by the processing map is Region I (350–500 °C, 1–10 s^{-1}), where the sample deformation is the most uniform and no cracks are generated.

3.4 Establishment of the constitutive equation for dysprosium

The parameters of hot deformation exert a crucial influence on the hot deformation behavior of alloys. This interrelation can be depicted using a constitutive relationship, specifically, a constitutive equation. In essence, the constitutive equation dynamically responds to the alterations in hot deformation parameters or state parameters (such as dislocation density and sub-grain size) by characterizing the flow stress of deformed materials. This study employs an Arrhenius-type equation, a phenomenological constitutive equation widely used in the field. This equation can be expressed in three forms: an exponential equation, a power function equation, and a hyperbolic sine equation. By conducting high-temperature compression tests, we obtained the true stress-true strain relationship curves for dysprosium. Furthermore, we discussed the impact of the amount of deformation, the temperature of deformation, and the strain rate on its hot deformation behavior.

Thermal deformation of metallic materials constitutes a thermally activated process. By examining the experimental data from high-temperature plastic deformation tests conducted on various materials, we discovered that the relationship between the flow stress of a material and its thermodynamic parameters can be represented using three forms of the Arrhenius equation.

$$\dot{\varepsilon} = A'\sigma_p^{n'} \exp\left(-\frac{Q}{RT}\right) \quad \alpha\sigma < 0.8 \text{ (low stress)} \tag{6}$$

$$\dot{\varepsilon} = A'' \exp(\beta\sigma_p) \exp\left(-\frac{Q}{RT}\right) \quad \alpha\sigma > 1.2 \text{ (high stress)} \tag{7}$$

$$\dot{\varepsilon} = A\left\{\sinh(\beta\sigma_p)\right\}^n \exp\left(-\frac{Q}{RT}\right) \quad \text{(applicable to all stress)} \tag{8}$$

In the equations, $\dot{\varepsilon}$ represents the strain rate, in s^{-1}; A is a constant; n is the stress exponent; σ_p is the peak stress, in Mpa; Q is the activation energy for thermal deformation, in kJ/mol; R is the gas constant, in J/K·mol; T is the absolute temperature, in K; α is the stress factor.

The true stress-true strain results indicate that the range of stress variation for dysprosium is substantial (0–300 MPa) following different deformation processes. Preliminary calculations reveal an approximate linear relationship between $\ln(\dot{\varepsilon})$ and $\ln(\sinh(\alpha\sigma))$, leading us to select the hyperbolic sine type Arrhenius equation to construct the constitutive relationship for dysprosium.

By taking the natural logarithm on both sides of Equations (6) and (7) and rearranging it, we derive the following equation:

$$\ln A' + n' \ln \sigma_p = \ln \dot{\varepsilon} + \frac{Q}{RT} \tag{9}$$

$$\ln A'' + \beta\sigma_p = \ln \dot{\varepsilon} + \frac{Q}{RT} \tag{10}$$

In accordance with Equations (9) and (10), the Origin software was used to perform linear fitting on $\ln \dot{\varepsilon}$ and $\ln \sigma_p$, as well as $\ln \dot{\varepsilon}$ and σ_p. The results are shown in **Figure 6**.

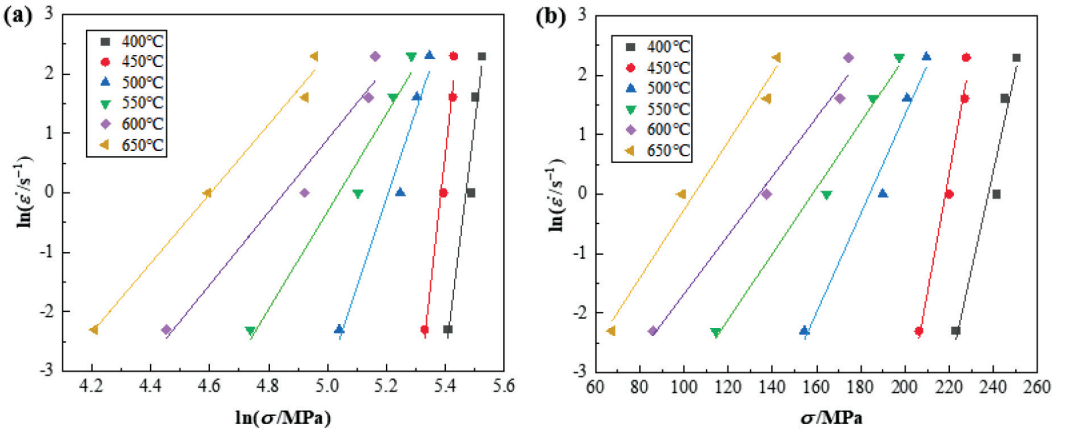

Figure 6: Fitting deformation parameters for different dysprosium processes: a) linear fitting of n' values, b) linear fitting of β values

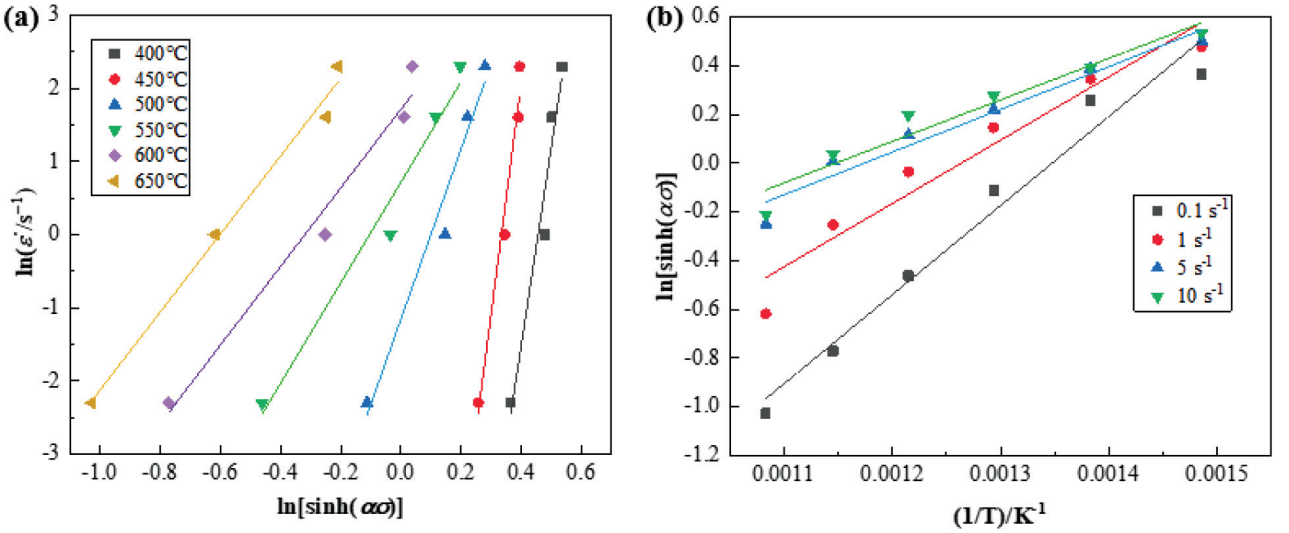

Figure 7: Fitting deformation parameters for different dysprosium processes: a) linear fitting of n values, b) linear fitting of Q/Rn values

The slopes of the linear fits give the values of n' and β as 19.7695 and 0.1029, respectively. Therefore, from the relationship between α, β, and n' in Equation (11), the value of α can be obtained as 0.0052.

$$\alpha = \frac{\beta}{n'} \tag{11}$$

Taking the logarithmic derivative of both sides of Equation (9) and rearranging it, we get Equation (12):

$$\ln \dot{\varepsilon} = \ln A + n \ln\left[\sinh(\alpha\sigma_{\mathrm{p}})\right]\left(-\frac{Q}{RT}\right) \tag{12}$$

Using data at the same deformation temperature, linear fitting is performed on ln[sinh($\alpha\sigma$p)] and ln$\dot{\varepsilon}$, as shown in **Figure 7a**. The slope of the line is the value of n, with an average value of 14.6827. When the strain rate is constant, ln[sinh($\alpha\sigma$p)] and 1/T are linearly fitted, as shown in **Figure 7b**. After fitting, the slope of the line is the value of Q/Rn. Taking the average of the fitting results of each line, the activation energy Q is obtained as 296.8929kJ/mol.

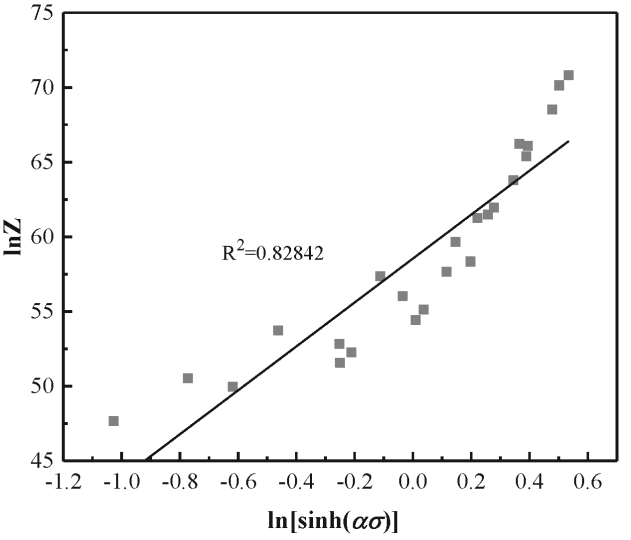

Figure 8: Linear relationship between ln[sinh(σp)] and ln Z for experimental steel

The Zener–Hollomon parameter (Z parameter) is referred to as the temperature-compensated strain rate factor. The expression for the Z parameter is shown in Equation (13):

$$Z = \dot{\varepsilon} \exp\left(-\frac{Q}{RT}\right) \tag{13}$$

The relationship between the Z parameter and the peak stress can be described by Equation (14):

$$Z = A\left[\sinh(\alpha\sigma_{\mathrm{p}})\right]^{n} \tag{14}$$

By taking the logarithm of both sides of Equations (2–9) and rearranging it, we obtain Equation (15):

$$\ln Z = \ln A + n \ln\left[\sinh(\alpha\sigma_{\mathrm{p}})\right] \tag{15}$$

To obtain the value of constant A, we should calculate the Z parameter through Equation (13), then perform the corresponding linear fit of ln Z and ln[sinh($\alpha\sigma_p$)]. The intercept value obtained is the value of ln$A$, from which we can determine the value of A. The fitting results are shown in **Figure 8**.

According to the linear fit, the intercept value, ln A, corresponds to $A = 2.6622 \times 10^{25}$. In summary, all the required parameter values are provided in **Table 1**.

Table 1: Parameters of empirical formula for thermal activation energy

n'	β	α	n	A	Q/KJ·mol^{-1}
19.7695	0.1029	0.0052	14.6827	2.6622×10^{25}	296.8929

By substituting the parameters from **Table 1** into Equation (8), we can obtain the constitutive equation for the relationship between the peak stress, deformation

temperature, and strain rate of dysprosium during hot processing:

$$e = 2.6622\times10^{25}\left[\sinh(0.0052\sigma)\right]^{14.6827}\cdot \cdot\exp\left(-\frac{296.8929}{8.314T}\right) \quad (16)$$

4 CONCLUSIONS

1) Single-pass hot simulation compression experiments were conducted using the MMS-200 thermal simulation testing machine. The true stress-true strain curves of dysprosium under different deformation processes were analyzed. As the strain rate increased to 5 s^{-1}, the curve gradually transitioned from dynamic recovery to dynamic recrystallization. As the strain rate increased, the softening behavior became more pronounced, which is consistent with the pattern found in high-purity fine-grain titanium.
2) By combining the processing map with the macro and micro morphology of the actual samples, it was found that the optimal processing area was located in Region I of the processing map: 350–500 °C, 1–10 s^{-1}. The deformation of the samples in this area was the most uniform, and no cracks were produced.
3) The Arrhenius equation, a widely used phenomenological constitutive equation, was adopted to establish the constitutive equation of dysprosium (Equation (16)).

Acknowledgment

The authors acknowledge the financial support from the Science and Technology Planning Project of Guangxi Province [AA22068083].

4 REFERENCES

[1] D. Wu, Z. Wang, D. Chen, et al., Research progress in preparation technology of high purity rare earth metals and alloy targets, Proceedings of the 2020 Academic Annual Meeting of the Chinese Society of Rare Earth and the Jiangxi (Ganzhou) Conference on Green Development and Efficient Utilization of Rare Earth Resources, 2020, 49–49

[2] Y. Wang, J. Gao, W. Li, et al., Study on thermal deformation behavior of Mg-Y-Nd-Zr rare earth magnesium alloys, 2008 Annual meeting of Chinese Mechanical Engineering Society and Gansu Province academic annual conference, 2008

[3] R. Ding, J. Zhou, X. Li, et al., Study on high temperature rheological behavior and hot working diagram of Ti-5Al-5Mo-5V-1Cr-1Fe titanium alloy, Forging and Stamping Technology, 44 (**2019**) 3, 7, doi:10.13330/j.issn.1000-3940.2019.03.021

[4] H. Wu, et al., Hot deformation behavior and constitutive equation of a new type Al-Zn-Mg-Er-Zr alloy during isothermal compression, Mater. Sci. Eng., A. Structural Materials: Properties, Microstructure and Processing, 651 (**2016**), 415–424, doi:10.1016/j.msea.2015.10.122

[5] W. Yao, et al., Hot Deformation Behavior and Microstructural Evolution of the As-Rolled 7050Al Alloy, Mater. Today. Commun., 38 (**2024**), 107861, doi:10.1016/j.mtcomm.2023.107861

[6] L. Liu, et al., Importance of cold rolling and tempering on the microstructure evolution, precipitation behavior and mechanical responses of 9Cr3Co3W1Cu ferritic/martensitic steel, Materials Characterization, 206 (**2023**), 113376, doi:10.1016/j.matchar.2023.113376

[7] L. Liu, et al., A heat-resistant steel with excellent high-temperature strength-ductility based on a combination of solid-solution strengthening and precipitation hardening, Materials Science and Engineering: A, 915 (**2024**), 147218, doi:10.1016/j.msea.2024.147218

[8] H. Mirzadeh, Constitutive modeling and prediction of hot deformation flow stress under dynamic recrystallization conditions, Mech. Mater., 85 (**2015**), 66–79, doi:10.1016/j.mechmat.2015.02.014

[9] A. Hunter, et al., Analytic model of dislocation density evolution in fcc polycrystals accounting for dislocation generation, storage, and dynamic recovery mechanisms, Int. J. Plast., 151 (**2022**), 103178, doi:10.1016/j.ijplas.2021.103178

[10] M. Rajamuthamilselvan, S. Ramanathan, Hot deformation behaviour of 7075 alloy, J. Alloys Compd., 509 (**2011**) 3, 948–952, doi:10.1016/j.jallcom.2010.09.139

[11] C. Zhang, C. Wang, R. Guo, et al., Investigation of dynamic recrystallization and modeling of microstructure evolution of an Al-Mg-Si aluminum alloy during high-temperature deformation, J. Alloys Compd., 773 (**2018**), 59–70, doi:10.1016/j.jallcom.2018.09.263

[12] A. Tekkaya, et al., Metal forming beyond shaping: Predicting and setting product properties, CIRP Annals, 64 (**2015**) 2, 629–653, doi:10.1016/j.cirp.2015.05.001

[13] T. Li, Sheet Preparation Technology, Microstructure and Properties of Hot-Pack Rolling Ti-44Al-5Nb-1Mo-2V-0.2B Alloys, Northeastern University, 2021

[14] Q. Jiang, Temperature effect on plastic deformation and damage behavior of ultra-fine crystalline pure metal materials, Northeastern University, 2011